https://dx.doi.org/10.4314/ijs.v25i2.4

ANALYSIS OF ELASTIC SCATTERING CROSS SECTIONS OF ^{16}O ON ^{27}Al AND ^{154}Sm USING THE SEMI-MICROSCOPIC DOUBLE FOLDING MODEL

Olorunfunmi, S. D. and Olatinwo, A. S.
Department of Physics and Engineering Physics, Obafemi Awolowo University, Ile-Ife, 220005, Osun State, Nigeria.
Corresponding Author's E-mail(s): sundayolorunfunmi@gmail.com; solorunfunmi@oauife.edu.ng
(Received: 1st April, 2023; Accepted: 28th July, 2023)

ABSTRACT

The elastic scattering data for ^{16}O + ^{27}Al at a laboratory energy (E_{Lab}) of 134 MeV and ^{16}O + ^{154}Sm at E_{Lab} = 85 and 134 MeV were analyzed using the optical model-based double-folding model. The real component of the optical model potential was generated from the microscopic double-folding (DF) model, while the imaginary part was considered using both microscopic and Woods-Saxon phenomenological forms. Two density-independent effective nucleon-nucleon (NN) interactions were considered in the DF procedure: the Michigan-3-Yukawa (M3Y) and Knyazkov and Hefter (KH). The folded potential was constructed using Two-parameter Fermi (2pF) density distribution for the target nuclei and three different forms of projectile density: Two-parameter Fermi (2pF), Slater determinants consisting of harmonic oscillator single-particle wave functions (SDHO), and Dirac-Hartree-Bogoliubov (DHB) density distributions. The SDHO density exhibited slightly better agreement with the data than 2pF and DHB. The results obtained using the KH interaction were highly consistent with those achieved with the M3Y interaction. In general, the DF model-based calculations compared reasonably well with the experimental data.

Keywords: Elastic scattering, Optical model, Double folding model, Density-independent potential.

INTRODUCTION

Nuclear reactions occur in various forms, such as elastic scattering, inelastic scattering, nucleon-transfer reaction, knock-out reaction, and others. These reactions can be described using different nuclear models. Elastic scattering is often investigated using the optical model (OM) approach, which involves a complex potential with real and imaginary parts. The real part represents the reflection of the projectile waves by the target nucleus, while the imaginary part describes their absorption.

When analyzing the elastic scattering data, the real and imaginary potentials can be represented in different forms. One form is the phenomenological approach, where both the real and imaginary potentials assume the Woods-Saxon (WS) shape. However, a major drawback of the phenomenological WS form is that it contains a large number of free parameters (at least six parameters), which leads to ambiguities. These parameter values are adjusted to provide an accurate fit to the elastic scattering data.

Another approach, with fewer free parameters and ambiguities, is to construct the real part of the OM potential using the double folding (DF) model and let the imaginary part assume a phenomenological WS form. The third approach is a complete microscopic form, where both the real and imaginary potentials are constructed from the DF model. In this last approach, the number of free parameters is very small, and consequently, the ambiguities are greatly reduced.

In the present study, we have employed the last two approaches. Specifically, in the DF model, the optical potential is obtained by folding a suitable effective nucleon-nucleon (NN) interaction over the density distributions of the two interacting nuclei (Satchler and Love, 1979). Some of the commonly used effective NN interactions are Michigan-3-Yukawa (M3Y) (Bertsch *et al.,* 1977), Knyazkov and Hefter (KH) (Knyazkov and Hefter,1981), Jeukenne, Lejeune and Mahaux (JLM) (1977), etc. Detailed review of the DF model is presented in Brandan *et al.,* (1997).

In recent years, there has been a renewed interest in multinucleon transfer reactions between heavy ions, particularly at energies around and above the Coulomb barrier (Corradi *et al.,* 2009; Zhang *et al.,* 2018; Sekizawa, 2019; Adamian *et al.,* 2020; Roy *et al.,* 2018; and Roy *et al.,* 2022). The study of

multinucleon transfer processes plays a crucial role in understanding nucleon-nucleon correlations and single-particle properties.

Recently, the elastic scattering and various transfer channels' angular distributions of ^{16}O on ^{27}Al at a laboratory energy of 134 MeV were measured using the Pelletron-LINAC accelerator facility in Mumbai, India (Roy *et al.,* 2022). Furthermore, using the same facility, Roy *et al.* (2018) measured the elastic scattering and many-nucleon transfer channels' angular distributions of ^{16}O on a well-deformed target nucleus, ^{154}Sm, at incident energies of 85 and 134 MeV, respectively, around and above the Coulomb barrier. Their primary objective was to investigate the effect of deformation on multinucleon transfer reactions.

The elastic-scattering data from both measurements were analyzed using the phenomenological optical model potential. Additionally, the many-nucleon transfer channels' angular distributions were analyzed using the time-dependent Hartree-Fock (TDHF) theory, along with a statistical model for secondary de-excitation processes, GEMINI++. However, it is important to note that the phenomenological WS potential is a simplified model that may not capture all the intricacies of the nuclear interaction. More advanced theoretical approaches, such as those based on microscopic DF models, are required to achieve a more comprehensive understanding of nuclear properties. The primary reason for choosing the DFM potential methods lies in their inherent advantages over the traditional phenomenological optical models. Firstly, the DF model approach provides a more realistic description of the nucleon-nucleus interaction by incorporating both the nucleon-nucleon (NN) and nucleus-nucleus (NA) interactions explicitly. This inclusion of microscopic NN interactions makes the DF model more accurate in predicting scattering observables in nuclear reactions. Secondly, the DF model has been successfully applied to various nuclear reactions (Khoa *et al.,* 2007; Olorunfunmi and Bahini, 2021) and has shown superior performance in reproducing experimental data. By employing a microscopic NN interaction model and considering the nuclear densities of both the projectile and target nuclei, the DF model offers a more comprehensive and reliable approach to analyze nuclear reactions compared to the phenomenological optical models.

The aim of this study is to reanalyze the recently measured ^{16}O + ^{27}Al (E_{Lab} = 134 MeV) (Roy *et al.,* 2018) and ^{16}O + ^{154}Sm (E_{Lab} = 85 and 134 MeV) (Roy *et al.,* 2022) elastic scattering data using the OM based DF model. Specifically, we will calculate the real component of the OM potential using DF model with two different forms of effective nuclear interactions: M3Y and KH. Additionally, we will consider both the microscopic and WS forms of the imaginary potential.

Furthermore, we aim to test the ability of three different projectile density distributions to describe the reactions considered.

MATERIALS AND METHODS

Double folding model

In the double folding model, the real part of the OM potential is usually expressed as

$$V_F(r) = \int dr_1 \int dr_2\, \rho_p(r_1)\rho_T(r_2)\upsilon_{NN}(|r_{12}|), \quad (1)$$

where r_{12} = [r - (r_1 - r_2)], ν_{NN} = effective NN interaction, ρ_p = density distribution of the projectile nucleus, and ρ_T = density distribution of the target nucleus.

Effective NN interaction

Two forms of effective NN interactions are considered in this study. The first is the popular density-independent M3Y interaction derived by Bertsch *et. al.,* and parametrized by Satchler and Love as,

$$\upsilon_{NN}^{M3Y} = 7999\frac{\exp(-4r)}{4r} - 2134\frac{\exp(-2.5r)}{2.5r} - 276\left[1 - 0.005\frac{E_{Lab}}{A_p}\right]\delta(r)\ \text{MeV}, \quad (2)$$

where E_{Lab} = laboratory energy in MeV, and A_p = mass number of the projectile.

The direct part of the interaction potential is represented by the first and second terms in equation (2), while the third term is the exchange

part estimated using a zero-range pseudopotential.

The second effective NN interaction is a Gaussian form of the effective NN interaction derived by Knyazkov and Hefter (1981) parametrized as follows:

$$v_{NN}^{KH}(r) = v_1 \exp(-r^2/a_1^2) + v_2 \exp(-r^2/a_2^2) - 276\left[1 - 0.005\frac{E_{Lab}}{A_p}\right]\delta(r), \quad (3)$$

where v_1 = -601.99 MeV, v_2 = 2256.4 MeV, a_1 = 0.8 fm and a_2 = 0.5 fm, and are taken from Knyazkov and Hefter, 1981.

Projectile density

In the present work, three different forms of density distributions are considered for the ^{16}O projectile nucleus. One of them is the Two-parameter Fermi (2pF) density distribution, which is expressed as follows (Seif and Mansour, 2015)

$$\rho_{n(p)}(r) = \rho_{0n(p)}\left[1 + \exp\left(\frac{r - R_{n(p)}}{a_{n(p)}}\right)\right]^{-1}, \quad (4)$$

where $R_n(R_p)$ = neutron (proton) half-density radius, and $a_n(a_p)$ = neutron (proton) surface thickness parameter.

These parameters are parameterized as follows (Seif and Mansour, 2015):

$$R_n = 0.953N^{1/3} + 0.015Z + 0.774; a_n = 0.446 + 0.0072\left(\frac{N}{Z}\right), \quad (5)$$

$$R_p = 1.322Z^{1/3} + 0.007N + 0.022; a_p = 0.449 + 0.0071\left(\frac{Z}{N}\right), \quad (6)$$

where N and Z are the neutron and proton numbers of the projectile nucleus. The second density distribution considered for ^{16}O projectile nucleus is the one obtained by Ahmad *et al.*, (2017) using the Slater determinants consisting of the harmonic oscillator single-particle wave functions. This is denoted as SDHO and parametrized as:

$$\rho_{n,p}^{16O}(r) = \frac{1}{\pi^{3/2}p^3}\left\{1 - \frac{3}{16a^2p^2} + \frac{r^2}{32a^2p^4}\right\}\exp\left(\frac{-r^2}{4p^2}\right), \quad (7)$$

where $a_p = \sqrt{0.286}$ fm, $a_n = \sqrt{0.295}$ fm, $p = \sqrt{\frac{A-1}{4a^2A}}$.

The quantity $a_p(a_n)$ is the oscillator parameter for the proton (neutron) and A is mass number of the nucleus.

The third projectile density distribution considered in this study is obtained from the Dirac-Hartree-Bogoliubov (DHB) model and is denoted as DHB, as described in Chamon *et al.,* (2002, 2021). Theoretical nuclear density distributions for a wide range of heavy-ion nuclei have been calculated by Chamon et al., (2002) using the Dirac-Hartree-Bogoliubov (DHB) model. A data file for DHB density distributions of a wide range of nuclei are used as input file for REGINA (Chamon et al., 2002) and are available online for public use. Detailed description of the DHB model and the calculation of the DHB density distribution can be found in Carlson and Hirata, (2000) and Chamon *et al.,* (2002), respectively. Figure 1 displays a comparative representation of the three density distributions for ^{16}O in both linear and logarithmic scales. The densities exhibit varying radial behavior, as evident from Figure 1(a). The DHB distribution is the largest at the nucleus center, while SDHO is the smallest. Both the DHB and SDHO density distributions show bumps in the central region, with peaks around 1.8 fm from the nucleus center. Figure 1(b) illustrates that at larger distances (r > 5.5 fm), the SDHO distribution is the smallest, while the 2pF distribution is the largest.

Target density

The density distribution of the target nuclei ^{27}Al and ^{154}Sm are taken to be two-parameter Fermi form

$$\rho(r) = \rho_0\left[1 + \exp\left(\frac{r - c}{z}\right)\right]^{-1}, \quad (8)$$

where c = 2.845 fm, z = 0.569 fm for ^{27}Al (Jager *et al.*, 1974), and c = 5.9387 fm, z = 0.522 fm for ^{154}Sm (De Vries *et al.*, 1987). The central density ρ_o can be obtained from the normalization condition:

$$4\pi\int \rho(r)r^2 dr = A \quad (9)$$

where A is the mass number of the nucleus.

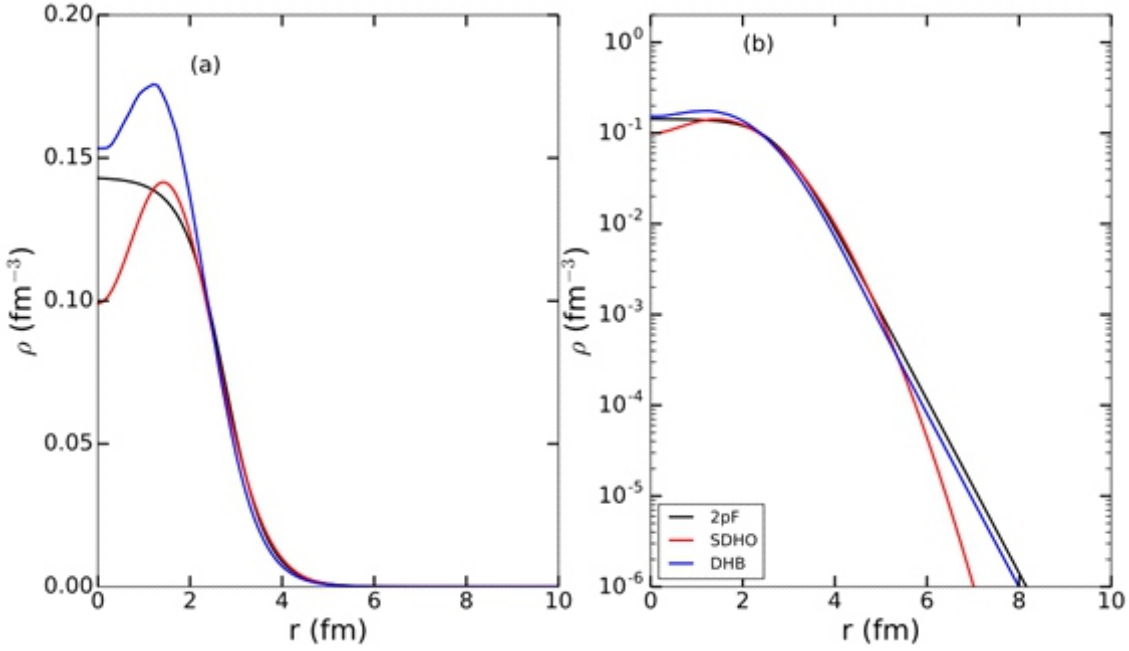

Figure 1: The 2pF, SDHO and DHB density distributions for ^{16}O in (a) linear scale and (b) logarithmic scale.

Method of calculation

Using the DFPOT code (Cook, 1982), the folded potentials for the projectile-target interactions are computed with the three different density distributions (2pF, SDHO, and DHB) together with each of the effective interactions. The folding process is conducted in momentum space, employing a Fourier transform technique. The resulting potentials obtained from DFPOT are then fed into the PTOLEMY code (Rhoades, 1980), which calculates the elastic scattering cross sections using the expression:

$$\frac{d\sigma}{d\Omega} = |f(\theta)|^2 , \quad (10)$$

Here, f (θ) is the elastic scattering amplitude, which is expressed as

$$f(\theta) = f_R(\theta) + (2ik)^{-1}\sum_l (2l+1)P_l(\cos\theta)(S_l - 1)e^{2i\delta_l}, \quad (11)$$

where θ, k, δ_l and S_l are the scattering angle, wave number, phase shift and scattering matrix element, respectively. The code performs the calculation using a total OM potential of the following form:

$$U(r) = V_c(r) - V(r) - iW(r), \quad (12)$$

where $V_c(r)$ = Coulomb potential, $V(r)$ = real volume potential, and $W(r)$ = imaginary volume potential.

The Coulomb potential is expressed as,

$$V_C(r) = \frac{1}{4\pi\varepsilon_o}\frac{Z_p Z_T e^2}{r}, r \geq R_C$$

$$= \frac{1}{4\pi\varepsilon_o}\frac{Z_p Z_T e^2}{2R_C}\left(3 - \frac{r^2}{R_C^2}\right), r < R_C \quad (13)$$

with

$$R_C = r_C\left(A_p^{(1/3)} + A_T^{(1/3)}\right), \quad (14)$$

Where $Z_p(Z_T)$ = projectile (target) charge, $A_P(A_T)$ = mass number of the projectile (target) nucleus, R_c = Coulomb radius of the optical potential, and r_c = the Coulomb radius parameter, which was set to 1.3 fm in this study.

The real component $V(r)$ of the OM potential is obtained using the double folding model as expressed in equation (1), with a renormalization factor N_R. The imaginary part of the potential is considered to be of two forms. The first one is the phenomenological WS form given by

$$W(r) = \frac{W_I}{1 + e^{\frac{r - r_I(A_p^{1/3} + A_T^{1/3})}{a_I}}}, \quad (15)$$

where W_1, r_1 and a_1 are the depth of the imaginary potential, the reduced radius, and the diffuseness parameter, respectively. In this case, the total OM potential (equation (12)) becomes

$$U(r) = V_C(r) - N_R V_F(r) - \mathrm{i}W(r). \quad (16)$$

For this case, we denote the total potentials as 2pF(R), SDHO(R) and DHB(R) using the density distributions 2pF, SDHO, and DHB, respectively, as ^{16}O density. The second one is the case where the imaginary phenomenological WS form is replaced with microscopic real folded potential. Then the total OM potential is expressed as

$$U(r) = V_C(r) - (N_R + \mathrm{i}N_I)V_F(r). \quad (17)$$

Similarly, for the second case, we denote the total potentials as 2pF(R+I), SDHO(R+I) and DHB(R+I) using the density distributions 2pF, SDHO, and DHB, respectively, as ^{16}O density.

To evaluate the level of agreement between the calculated results and experimental data, the imaginary reduced radius r_1 and diffuseness a_1 were held constant at 1.2518 fm and 0.601 fm, respectively, and a search on the depth of the imaginary potential (W_1) and the renormalization constants (N_R and N_I) was carried out using the reduced chi-square :

$$\frac{\chi^2}{N} = \sum_{k=1}^{N}\left[\frac{\sigma_{\mathrm{cal}}(\theta_k) - \sigma_{\mathrm{ex}}(\theta_k)}{\Delta\sigma_{\mathrm{ex}}(\theta_k)}\right]^2. \quad (18)$$

Here, $\sigma_{cal}(\theta_k)$ = theoretical cross section,
$\sigma_{ex}(\theta_k)$ = experimental cross sections,
$\Delta\sigma_{ex}(\theta_k)$ = experimental error, and
N = number of data points.

In the study of elastic scattering cross sections, the volume integral is an important quantity, as it provides information about the nuclear density distribution and the interaction between interacting nuclei. In this study, we calculated the real (J_R) and imaginary (J_I) volume integrals using the formulae (Satchler and Love, 1979):

$$J_R(E) = \frac{-4\pi}{A_p A_T}\int V(r,E)r^2\mathrm{d}r, \quad (19)$$

and

$$J_I(E) = \frac{-4\pi}{A_p A_T}\int W(r,E)r^2\mathrm{d}r. \quad (20)$$

Finally, the root mean square radius of the DF potential is obtained from the expression (Varner *et al.*, 1991):

$$\langle r^2\rangle^{1/2} = \sqrt{\frac{\int V_F(r)r^4\mathrm{d}r}{\int V_F(r)r^2\mathrm{d}r}}. \quad (21)$$

The rms radius of nucleus is an important quantity in nuclear physics that provides information about the size and structure of the nucleus.

RESULTS AND DISCUSSION

The DF model is used to calculate the real part of the optical potentials for the ^{16}O + ^{27}Al reaction at 134 MeV and the ^{16}O + ^{154}Sm reaction at 85 and 134 MeV, with M3Y and KH effective interactions and three different forms of projectile densities (2pF, SDHO and DHB). Figures 2 and 3 show the typical calculated DF potentials for ^{16}O + ^{27}Al and ^{16}O + ^{154}Sm at 134 MeV, respectively, using the aforementioned interactions and densities. It can be observed that the M3Y and KH interactions produce DF potentials with similar depths and shapes. Furthermore, the DF potential obtained from the DHB density has a slightly deeper depth than that obtained from the 2pF and SDHO distributions. This is because the DHB gives the highest density value at the center of the nucleus compared to the other two densities as shown in Figure 1(a).

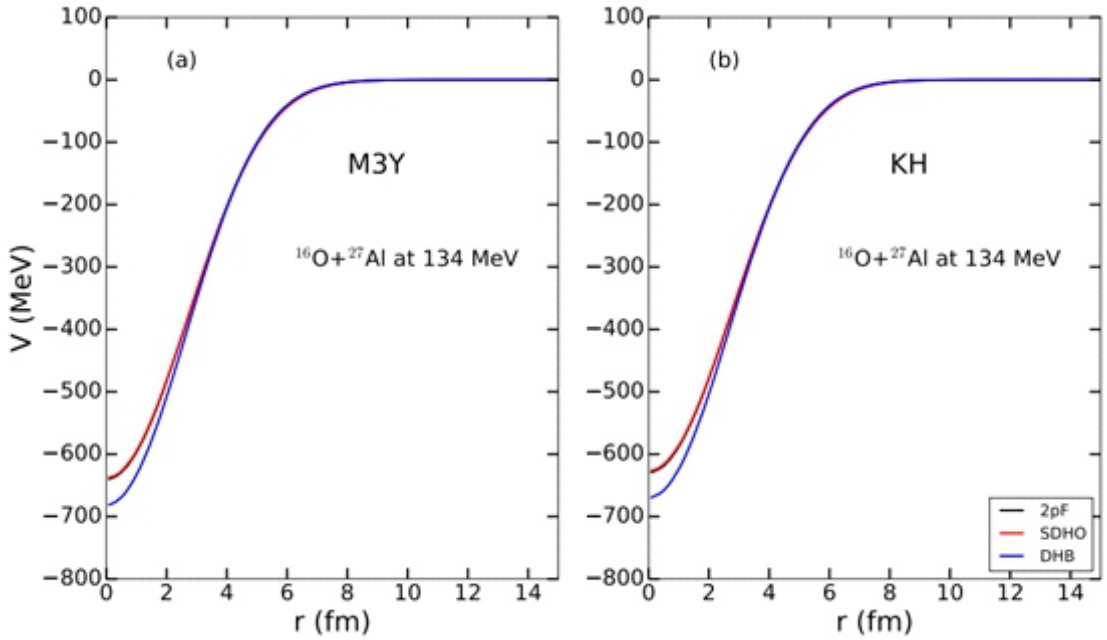

Figure 2: Real folded potentials for ^{16}O+^{27}Al at 134 MeV using 2pF, SDHO and DHB density distributions with (a) M3Y and (b) KH effective interactions.

Table 1 presents the root mean square (rms) radii, denoted as $\langle r^2_{M3Y}\rangle^{1/2}$ and $\langle r^2_{\mathrm{KH}}\rangle^{1/2}$, calculated for the DF potentials using M3Y and KH interactions with the 2pF, SDHO, and DHB densities. As shown in the table, the rms radius of the DF potential obtained from DHB is smaller than that for the 2pF and SDHO densities. The difference is about one percent, hence, it is of no consequence. Additionally, we observe that the rms radii increase as the mass number increases for all densities. It is worth noting that the rms radii obtained with the M3Y interaction display a behavior and value that are apparently similar to those obtained with the KH interaction.

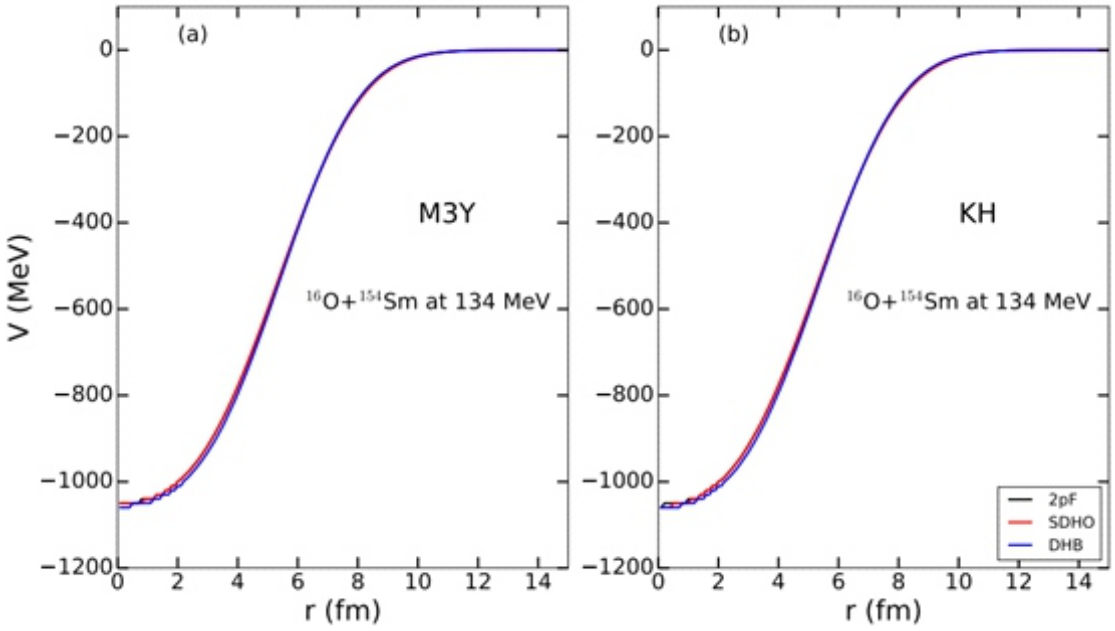

Figure 3: Same as Figure 2 but for ^{16}O+^{154}Sm at 134 MeV.

Table 1: Root mean square radii $<r^2>^{1/2}$ of the calculated DF potentials with M3Y and KH effective interactions, and three densities (2pF, SDHO and DHB) for ^{16}O + ^{27}Al and ^{16}O + ^{154}Sm reactions.

System	Energy (MeV)	Density	$< r^2_{M3Y} >^{1/2}$ (fm)	$< r^2_{KH} >^{1/2}$ (fm)
^{16}O+^{27}Al	134	2pF	4.396	4.396
		SDHO	4.395	4.395
		DHB	4.313	4.313
^{16}O + ^{154}Sm	85	2pF	5.906	5.906
		SDHO	5.906	5.906
		DHB	5.845	5.845
^{16}O + ^{154}Sm	134	2pF	5.908	5.908
		SDHO	5.908	5.908
		DHB	5.847	5.847

To compute the elastic scattering cross sections using M3Y and KH, two methods were utilized. Method one employs a microscopic folded potential for both the real and imaginary components of the nuclear potential. In method two, a folded potential is used for the real part while the imaginary part is modeled using the Woods-Saxon form. The calculated results based on the 2pF, SDHO, and DHB density distributions with folded real and imaginary Woods-Saxon potentials are labeled as 2pF(R), SDHO(R), and DHB(R), respectively. The calculated results based on the 2pF, SDHO, and DHB density distributions with folded real and imaginary potentials are labeled as 2pF(R+I), SDHO(R+I), and DHB(R+I), respectively.

The elastic scattering cross sections of the ^{16}O + ^{27}Al and ^{16}O + ^{154}Sm reactions at 134 MeV and 85 MeV, respectively, were computed using the potentials 2pF(R), SDHO(R), DHB(R), 2pF(R+I), SDHO(R+I), and DHB(R+I) with both M3Y and KH interactions. The resulting elastic scattering cross sections normalized to Rutherford cross sections σ_{Ruth} were compared to experimental data and presented in Figures 4 to 6. Tables 2 and 3 show the values of N_R, N_I, J_R, J_I, W_I, σ_I and X^2/N, that produced good agreement with the data.

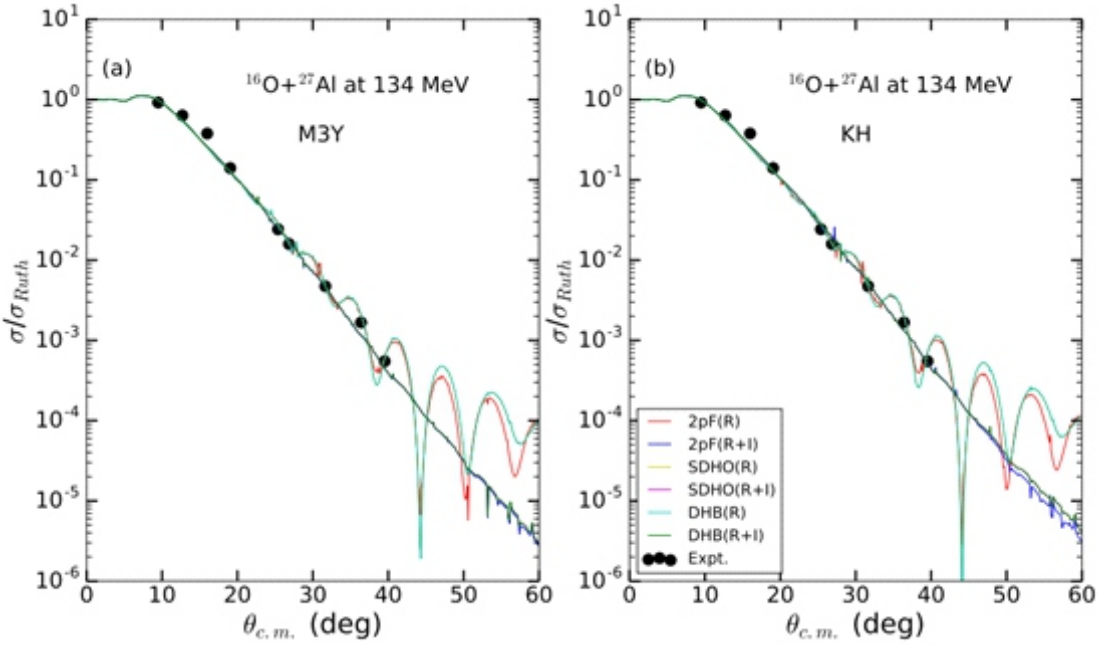

Figure 4: Elastic scattering cross sections for ^{16}O+^{27}Al at 134 MeV calculated using 2pF, SDHO and DHB projectile densities with (a) M3Y and (b) KH interactions. The experimental data are taken from Roy *et al.*, 2018.

Table 2: Real renormalization constants (N_R), depth of the imaginary potential, real and volume integrals (J_R and J_I), total reaction cross sections (σ) and X^2/N values for $^{16}O+^{27}Al$ and $^{16}O+^{154}Sm$ elastic scattering using the M3Y and KH potentials. The imaginary radius r_I and diffuseness a_I are fixed at 1.2518 fm and 0.601 fm, respectively.

System	Energy (MeV)	Potential	Density	N_R	W_I (MeV)	J_R (MeV fm^3)	J_I (MeV fm^3)	χ^2/N	σ_R (mb)
$^{16}O+^{27}Al$	134	M3Y	2pF	0.15	8.469	61.52	29.12	2.60	1588.4
			SDHO	0.15	8.30	61.52	28.53	2.58	1582.1
			DHB	0.15	8.20	82.02	28.19	4.30	1575.5
		KH	2pF	0.15	8.40	61.52	28.88	3.14	1586.0
			SDHO	0.15	8.20	61.52	28.19	2.99	1578.5
			DHB	0.15	8.00	82.03	27.50	5.07	1567.9
$^{16}O+^{154}Sm$	85	M3Y	2pF	0.7	24.00	290.0	40.59	1.06	1109.3
			SDHO	0.7	24.0	290.0	40.59	1.05	1107.2
			DHB	0.8	24.0	331.5	40.59	1.05	1107.1
		KH	2pF	0.8	16.56	331.5	28.03	1.77	1033.7
			SDHO	0.8	24.0	331.5	40.59	1.09	1110.3
			DHB	1.0	20.0	331.4	33.83	1.46	1077.1
$^{16}O+^{154}Sm$	134	M3Y	2pF	1.0	24.21	410.1	40.95	1.00	2290.9
			SDHO	1.1	24.00	451.1	40.59	0.94	2294.9
			DHB	1.25	24.00	512.6	40.59	0.92	2294.2
		KH	2pF	1.0	18.47	410.1	31.24	1.98	2210.8
			SDHO	1.15	24.00	471.6	40.59	1.13	2292.4
			DHB	1.25	24.00	512.6	40.59	1.58	2287.0

Table 3: Real and imaginary renormalization constants (N_R *and* N_I), real and imaginary volume integrals (J_R and J_I), total reaction cross sections (σ) and X^2/N values for $^{16}O+^{27}Al$ and $^{16}O+^{154}Sm$ elastic scattering using the M3Y potential.

System	Energy (MeV)	Potential	Density	N_R	N_I	J_R (MeV fm^3)	J_I (MeV fm^3)	χ^2/N	σ_R (mb)
$^{16}O+^{27}Al$	134	M3Y	2pF	0.15	0.25	61.52	102.53	3.17	1588.1
			SDHO	0.15	0.25	61.52	102.53	3.11	1587.1
			DHB	0.2	0.32	82.02	131.24	2.73	1584.8
		KH	2pF	0.15	0.25	61.52	102.53	2.71	1571.5
			SDHO	0.15	0.25	61.52	102.54	2.81	1564.2
			DHB	0.2	0.3	82.03	123.04	2.70	1587.9
$^{16}O+^{154}Sm$	85	M3Y	2pF	0.6	1.0	248.61	414.36	1.07	1179.1
			SDHO	0.7	0.9	290.06	372.94	1.04	1134.4
			DHB	0.8	1.0	331.51	414.38	1.03	1135.8
		KH	2pF	0.8	1.0	331.51	414.39	1.27	1147.1
			SDHO	0.8	1.0	331.47	414.34	1.02	1115.1
			DHB	1.0	1.0	414.33	414.33	1.20	1102.1
$^{16}O+^{154}Sm$	134	M3Y	2pF	1.0	1.0	410.13	410.13	0.95	2384.6
			SDHO	1.1	1.0	451.16	410.15	0.91	2360.9
			DHB	1.3	1.0	533.17	410.13	0.89	2334.2
		KH	2pF	1.1	1.0	451.16	410.15	1.29	2338.3
			SDHO	1.3	1.0	533.22	410.17	0.94	2318.3
			DHB	1.4	1.0	574.20	410.14	1.05	2286.9

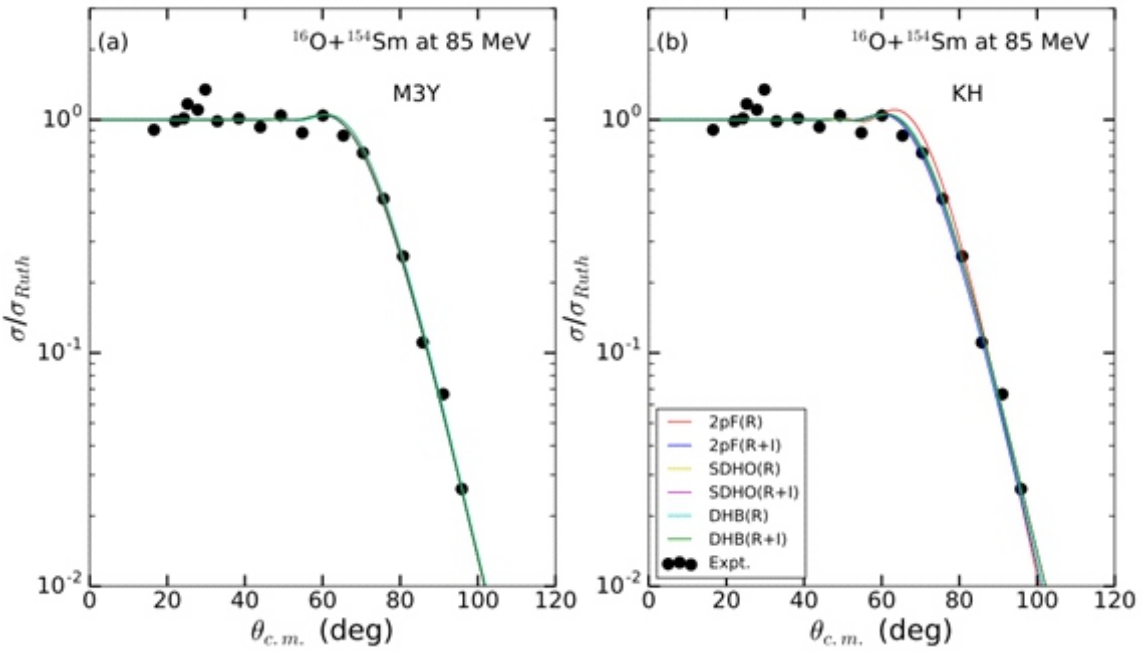

Figure 5: Same as Figure 4 but for ^{16}O+^{154}Sm at 85 MeV. The experimental data are taken from Roy *et al.*, 2022.

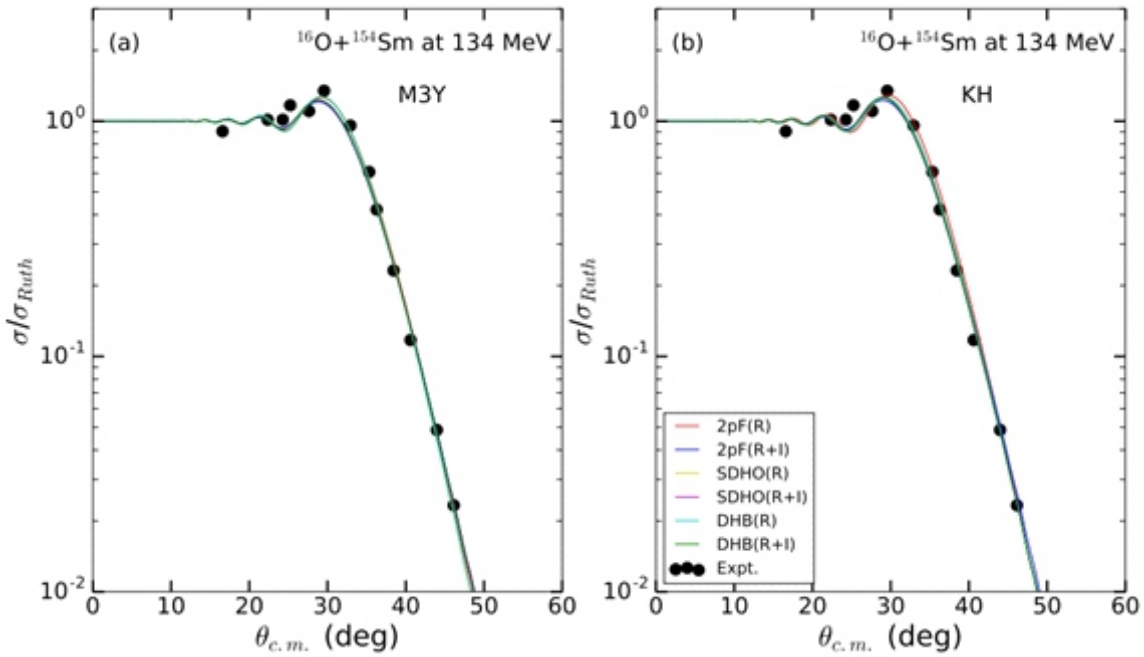

Figure 6: Same as Figure 4 but for ^{16}O+^{154}Sm at 134 MeV. The experimental data are taken from Roy *et al.*, 2022.

Figure 4 illustrates the results obtained for the ^{16}O + ^{27}Al system at 134 MeV with M3Y and KH interactions. The calculated results show a reasonable agreement with the experimental data. However, Tables 2 and 3 indicate that, for the three densities (2pF, SDHO, and DHO), the values of the renormalization constants (N_R and N_I) required for the DF potentials to reproduce the experimental data successfully are significantly different from unity. The interactions with very low N_R and N_I are too deep or strong. . This might be attributed to the nature of the experimental data. Additionally, the experimental data in Figure 4 covers only a limited range of angles, $\theta_{c.m.} \approx 10^{o}$ - 40^{o}. Consequently, it is advisable to measure data at larger angles to study the realistic effect of the considered potentials on the elastic scattering results. Moreover, the values of σ_R obtained for the ^{16}O + ^{27}Al system in this study are approximately 15% higher on average than those obtained using phenomenological potentials in Ref. (Roy, 2018).

We present the results of our analysis of two data sets for the ^{16}O + ^{154}Sm system at energies of 85 and 134 MeV in Figures 5 and 6, respectively. Figures 5(a) and 6(a) show the results obtained with the M3Y interaction, while Figures 5(b) and 6(b) show those obtained with the KH interaction. It can be observed that the elastic scattering cross sections obtained with all the densities and their corresponding DF potentials are in good agreement with the data. Additionally, Tables 2 and 3 reveal that all densities yield comparable values of x^2/N at both energies. Although, the DHB density slightly performs best. Moreover, we note that the values N_R of increase from the range 0.7 to 1.0 at 85 MeV to approximately 1.0 to 1.3 at 134 MeV. Furthermore, the values of σ_R increase by around 100% as the incident energy increases from 85 MeV to 134 MeV, which is expected. Finally, the values of σ_R obtained in this study using the DF model are in close agreement with those obtained using phenomenological potentials (σ_R = 1182 and 2357 mb) (Roy *et al.*, 2022) with a difference of less than 5%.

After analyzing the M3Y and KH effective interactions, we found that both interactions require nearly the same renormalization constant to describe the experimental data, as shown in Tables 2 and 3. Moreover, the values of σ_R for M3Y are slightly higher than those for the KH interaction. We also observed that both interactions provide similar fits to the data, which is evident from the values of x^2/N presented in Tables 2 and 3. Interestingly, all the density distributions for each effective interaction provide comparable quality of fits, with only a $\sim$ 5% variation in the reaction cross-sections and similar behavior of the potential renormalization factors. However, the DHB density distribution performs best.

CONCLUSION

DF optical model potentials were developed using M3Y and KH interactions, and three distinct projectile density forms, namely 2pF, SDHO, and DHB. These potentials were then employed to study elastic scattering data for ^{16}O + ^{27}Al at 134 MeV and ^{16}O + ^{154}Sm at 85 and 134 MeV. Two forms of the imaginary potential, namely the microscopic and the phenomenological WS forms, were examined. The results indicated that the 2pF, SDHO, and DHB densities produced good agreement with the experimental data, but the DHB density demonstrated superior performance as measured by the chi-square value.

Overall, the DF elastic scattering cross sections computed using the M3Y and KH effective interactions exhibit reasonable agreement with the experimental data across all the reactions analyzed. These results suggest that the double folding potentials, which only involve a small number of fitting parameters, offer a satisfactory representation of the data. This reinforces the advantage of the DF model-based optical potential over the phenomenological form, which typically demands a greater number of fitting parameters.

DECLARATION OF CONFLICT OF INTEREST

Not applicable.

REFERENCES

Adamian, G.G., Antonenko, N.V., Diaz-Torres, A. and Heinz, S. 2020. How to extend the chart of nuclides? *The European Physical Journal A* 56 (2): 47. doi:10.1140/epja/s10050-020-00046-7

Ahmad, S., Usmani, A.A., Ahmad, S., and Khan, Z.A. 2017. Interaction cross sections and matter radii of oxygen isotopes using the Glauber model. *Physical Review C* 95 (5): 054601. doi:10.1103/PhysRevC.95.054601

Bertsch, G., Borysowicz, J., H. McManus, H. and W. G. Love, W. G. 1977. Interactions for inelastic scattering derived from realistic potentials. *Nuclear Physics A* 284 (5): 399 - 419. doi:10.1016/0375-9474(77)90392-X

Brandan, M. E. and Satchler, G. R. 1997. The interaction between light heavy-ions and what it tells us. *Physics Reports* 285 (4 - 5): 142 – 243. doi:10.1016/S0370-1573(96)00048-8

Carlson, B. V. and Hirata, D. 2000. Dirac-Hartree-Bogoliubov approximation for finite nuclei. *Physical Review C 62 (5): 054310.* doi:10.1103/PhysRevC.62.054310

Chamon, L.C., Carlson, B.V., Gasques, L.R. 2021. Sao Paulo potential version 2 (SPP2) and Brazilian nuclear potential (BNP). *Computer Physics Communications* 267 (10): 108061. doi: 10.1016/j.cpc.2021.108061

Chamon, L.C., Carlson, B.V., Gasques, L.R., Pereira, D., De Conti, C., Alvarez, M.A.G., Hussein,M.S., Candido Ribeiro, M.A., Rossi, E.S., Jr. Silva, C.P. 2002. Toward a global description of the nucleus-nucleus interaction. *Physical Review C* 66 (1): 014610. doi:10.1103/PhysRevC.66.014610

Cook, J. 1982. DFPOT - A program for the calculation of double folded potentials. *Computer Physics Communications* 25 (2): 125 - 139. doi:10.1016/0010-4655(82)90029-7

Corradi, L., Pollarolo, G., and Szilner, S. 2009. Multinucleon transfer processes in heavy-ion reactions. *Journal of Physics G, Nuclear and Particle Physics* 36 (11): 113101. doi:10.1088/0954-3899/36/11/113101

De Jager, C.W., De Vries, H. and De Vries, C. 1974. Nuclear charge- and magnetization-density-distribution parameters from elastic electron scattering. *Atomic Data and Nuclear Data Tables* 14 (5 – 6): 479 - 508. doi:10.1016/S0092-640X(74)80002-1

De Vries, H., De Jager, C.W., and De Vries, C. 1987. Nuclear charge-density-distribution parameters from elastic electron scattering. *Atomic Data and Nuclear Data Tables* 36 (3): 495 - 536. doi:10.1016/0092-640X(87)90013-1

Jeukenne, J.P., Lejeunne, A., Mahaux, C. 1977. Optical-model potential in finite nuclei from Reid's hard core interaction. *Physical Review C* 16 (1): 80. doi:10.1103/PhysRevC.16.80

Knyazkov, O.M., Hefter, E.F. 1981. An analytical folding potential for deformed nuclei. *Zeitschrift für Physik A* 301 (3): 277 - 282. doi:10.1007/BF01416304

Khoa, D.T., von Oertzen W., Bohlen, H.G., and Ohkubo, S. 2007. Nuclear rainbow scattering and nucleus–nucleus potential. *Journal of Physics G, Nuclear and Particle Physics* 34 (3): R111–R164. doi: 10.1088/0954-3899/34/3/R01

Olorunfunmi, S. D. and Bahini, A. 2021. Microscopic Analysis of Elastic Scattering Angular Distributions for Five Different Density Distribution of ^{9}Be Nucleus. *Physics of Atomic Nuclei,* 84 (4): 448–459. doi: 10.1134/S1063778821040244

Rhoades-Brown, M., Macfarlane, M. H.and S. C. Pieper, S. C. 1980. Techniques for heavy-ion coupled-channels calculations. I. Long-range Coulomb coupling. *Physical Review C* 21 (6): 2417 - 2426. doi:10.1103/PhysRevC.21.2417

Roy, B.J., Sawant, Y., Patwari, P., Santra, S., Pal, A., Kundu, A., Chattopadhyay, D., Jha, V., Pandit, S.K., Parkar, V.V., Ramachandran, K., Mahata, K., Nayak, B.K., Saxena, A., Kailas,S., Nag, T.N., Sahoo, R.N., Singh, P.P. and Sekizawa, K. 2018. Deep--inelastic multinucleon transfer processes in the ^{16}O+^{27}Al reaction. *Physical Review C* 97 (3): 034603. doi:10.1103/PhysRevC.97.034603

Roy, B.J., Santra, S., Pal, A., Kumawat, H., Pandit, S.K., Parkar, V.V., Ramachandran, K. Mahata, K. and Sekizawa, K. 2022. Reaction mechanism study for multinucleon transfer processes in collisions of spherical and deformed nuclei at energies near and above the Coulomb barrier: The $^{16}O+^{154}Sm$ reaction. *Physical Review C* 105 (4): 044611. doi:10.1103/PhysRevC.105.044611

Satchler, G. R. and Love, W. G. 1979. Folding model potentials from realistic interactions for heavy-ion scattering. *Physics Reports* 55 (3): 183 - 254. doi:10.1016/0370-1573(79)90081-4

Seif, W.M. and Mansour, H. 2015. Interaction cross sections and matter radii of oxygen isotopes using the Glauber model. *International Journal of Modern Physics E* 24 (11): 1550083. doi:10.1142/S0218301315500834

Sekizawa, K. 2019. Time-dependent Hartree-Fock theory and its extensions for the multinucleon transfer reactions: A mini review. *Frontiers of Physics* 7 (20): 1 - 11. doi:10.3389/fphy.2019.00020

Varner, R. L., Thompson, W. J., McAbee, T. L., Ludwig, E. J. and T. B. Clegg, T. B. 1991. A global nucleon optical model potential. *Physics Reports* 201 (2): 57 - 119. doi:10.1016/0370-1573(91)90039-O.

Zhang, F.S., Li, C., Zhu, L., and Wen, P. 2018. Production cross sections for exotic nuclei with multinucleon transfer reactions. Frontiers of Physics 13 (6): 132113. doi:10.1007/s11467-018-0843-6